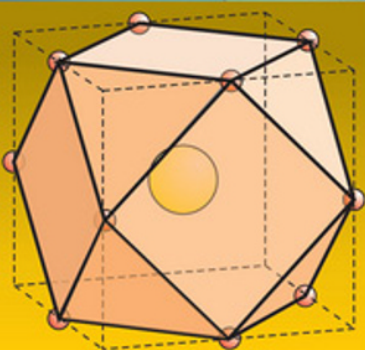


Richard J.D. Tilley

PEROVSKITES

Structure–Property Relationships



WILEY

Perovskites

Perovskites

Structure–Property Relationships

RICHARD J. D. TILLEY

Professor Emeritus, Cardiff University, UK

WILEY

This edition first published 2016
© 2016 John Wiley & Sons, Ltd

First Edition published in 2016

Registered Office

John Wiley & Sons, Ltd, The Atrium, Southern Gate, Chichester, West Sussex, PO19 8SQ, United Kingdom

For details of our global editorial offices, for customer services and for information about how to apply for permission to reuse the copyright material in this book please see our website at www.wiley.com.

The right of the author to be identified as the author of this work has been asserted in accordance with the Copyright, Designs and Patents Act 1988.

All rights reserved. No part of this publication may be reproduced, stored in a retrieval system, or transmitted, in any form or by any means, electronic, mechanical, photocopying, recording or otherwise, except as permitted by the UK Copyright, Designs and Patents Act 1988, without the prior permission of the publisher.

Wiley also publishes its books in a variety of electronic formats. Some content that appears in print may not be available in electronic books.

Designations used by companies to distinguish their products are often claimed as trademarks. All brand names and product names used in this book are trade names, service marks, trademarks or registered trademarks of their respective owners. The publisher is not associated with any product or vendor mentioned in this book.

Limit of Liability/Disclaimer of Warranty: While the publisher and author have used their best efforts in preparing this book, they make no representations or warranties with respect to the accuracy or completeness of the contents of this book and specifically disclaim any implied warranties of merchantability or fitness for a particular purpose. It is sold on the understanding that the publisher is not engaged in rendering professional services and neither the publisher nor the author shall be liable for damages arising herefrom. If professional advice or other expert assistance is required, the services of a competent professional should be sought.

Library of Congress Cataloging-in-Publication data applied for

ISBN: 9781118935668

A catalogue record for this book is available from the British Library.

Set in 10.5/13.5pt Times by SPi Global, Pondicherry, India

Contents

<i>Preface</i>	xi
1 The ABX_3 Perovskite Structure	1
1.1 Perovskites	1
1.2 The Cubic Perovskite Structure: $SrTiO_3$	4
1.3 The Goldschmidt Tolerance Factor	6
1.4 ABX_3 Perovskite Structure Variants	11
1.5 Cation Displacement: $BaTiO_3$ as an Example	12
1.6 Jahn–Teller Octahedral Distortion: $KCuF_3$ as an Example	16
1.7 Octahedral Tilting	19
1.7.1 Tilt Descriptions	19
1.7.2 Trigonal Symmetry: $LaAlO_3$ as an Example	24
1.7.3 Orthorhombic Symmetry: $GdFeO_3$ and $CaTiO_3$ as Examples	26
1.8 Symmetry Relationships	30
1.9 Hybrid Organic–Inorganic Perovskites	33
1.10 Antiperovskites	34
1.10.1 Cubic and Related Structures	34
1.10.2 Other Structures	36
1.11 Structure-Field Maps	36
1.12 Theoretical Calculations	38
References	40
Further Reading	40
2 ABX_3–Related Structures	42
2.1 Double Perovskites and Related Ordered Structures	42
2.1.1 Rock-Salt Ordered Double Perovskites	42
2.1.2 Other Ordered Perovskites	45
2.1.3 $AA'_3B_4O_{12}$ -Related Phases	48

2.2	Anion Substituted Perovskites	51
2.2.1	Nitrides and Oxynitrides	51
2.2.2	Oxyfluorides	53
2.3	A-Site-Deficient Perovskite Structures	54
2.3.1	ReO_3 , WO_3 and Related Structures	54
2.3.2	Perovskite Tungsten Bronzes	55
2.3.3	A-Site-Deficient Titanates, Niobates and Tantalates	55
2.4	Anion-Deficient Phases Containing Tetrahedra	57
2.4.1	Brownmillerites	57
2.4.2	Brownmillerite Microstructures	62
2.4.3	Temperature Variation and Disorder	63
2.4.4	B-Site Doped Brownmillerite Phases	64
2.4.5	B-Site Doping and Oxygen Pressure	65
2.4.6	A-Site Doped Brownmillerite Phases	65
2.4.7	Brownmillerite-Related Phases	66
2.5	Anion-Deficient Phases Containing Square Pyramids	69
2.5.1	Manganites	69
2.5.2	$\text{SrFeO}_{2.5}$ and Related Phases	71
2.5.3	Cobaltite-Related Phases	73
2.6	Point Defects, Microdomains and Modulated Phases	74
	Further Reading	78
3	Hexagonal Perovskite-Related Structures	79
3.1	The BaNiO_3 Structure	79
3.2	BaNiO_3 -Related Phases Containing Trigonal Prisms	81
3.2.1	Commensurate Structures	81
3.2.2	Modulated Structures	89
3.3	Perovskites with Mixed Hexagonal/Cubic Packing: Nomenclature	92
3.4	Perovskites with Mixed Hexagonal/Cubic Packing: Stacking Sequences	95
3.5	Hexagonal Perovskites with ch_q and c_ph Stacking	98
3.5.1	(ch_q) Structures	98
3.5.2	(c_ph) Structures	99
3.5.3	c_ph_q Intergrowth Structures	104
3.6	Hexagonal Perovskites with c_phh Stacking	106
3.6.1	$(\text{cc}\dots\text{chh}) \text{A}_n\text{B}_n\text{O}_{3n}$ Structures	107
3.6.2	$(\text{cc}\dots\text{chh}) \text{A}_n\text{B}_{n-1}\text{O}_{3n}$ Structures	108
3.6.3	$(\text{hhcc}\dots\text{chhcc}\dots\text{c})$ Intergrowth Phases	110

3.6.4	(cc...ch) $A_nB_{n-1}O_{3n}$ Shift and Twinned Phases	112
3.7	Anion-Deficient Phases Containing BaO_2 (c') Layers	112
3.7.1	(c...c'...ch) Structures	113
3.7.2	(c...c'...chh) Structures	113
3.7.3	(c...c'...chhh) Structures	115
3.8	Anion-Deficient Phases with $BaOX$ Layers	117
3.8.1	(h') Layers	117
3.8.2	(c'c') Layers	119
3.9	$Sr_4Mn_3O_{10}$ and $Ba_6Mn_5O_{16}$	120
3.10	Temperature and Pressure Variation	120
	Reference	122
	Further Reading	122
4	Modular Structures	123
4.1	K_2NiF_4 (A_2BX_4) and Ruddlesden–Popper Phases	123
4.1.1	The K_2NiF_4 (T or T/O) Structure	123
4.1.2	Ruddlesden–Popper Phases	127
4.2	The Nd_2CuO_4 (T') and T* Structures	129
4.3	Dion–Jacobson and Related Phases	131
4.4	Aurivillius Phases	134
4.5	The $Ca_2Nb_2O_7$ -Related Phases	136
4.6	Cuprate Superconductors and Related Phases	138
4.6.1	La_2CuO_4 , Nd_2CuO_4 and $YBa_2Cu_3O_7$	139
4.6.2	Layered Perovskite Structures	141
4.6.3	Structures Related to the Layered Cuprate Phases	142
4.7	Composition Variation	146
4.8	Intercalation and Exfoliation	151
	Further Reading	154
5	Diffusion and Ionic Conductivity	156
5.1	Diffusion	156
5.2	Ionic Conductivity	159
5.3	Proton Conductivity	162
5.4	Oxygen Pressure Dependence and Electronic Conductivity	165
5.5	Oxide Ion Mixed Conductors	167
5.6	Proton Mixed Conductors	169
5.7	Solid Oxide Fuel Cells	172
	References	174
	Further Reading	174

6	Dielectric Properties	176
6.1	Insulating Perovskites	176
6.2	Dielectric Perovskites	178
6.2.1	General Properties	178
6.2.2	Colossal Dielectric Constant Materials	181
6.3	Ferroelectric/Piezoelectric Perovskites	182
6.3.1	Spontaneous Polarisation and Domains	182
6.3.2	Ferroelectric Domain Switching	185
6.3.3	Ferroelectric Hysteresis Loops	188
6.3.4	Temperature Dependence of Ferroelectricity	189
6.3.5	Pyroelectrics, Piezoelectrics and Crystal Symmetry	191
6.3.6	Strain versus Electric Field Loops	192
6.4	The Development of Ferroelectric/Piezoelectric Ceramic Bodies	193
6.4.1	Ceramic Piezoelectrics	193
6.4.2	Electrostriction	195
6.5	Antiferroelectrics	196
6.6	Ferrielectrics	199
6.7	Relaxor Ferroelectrics	200
6.7.1	Macroscopic Characteristics of Relaxor Ferroelectrics	200
6.7.2	Microstructures of Relaxor Ferroelectrics	202
6.8	Improper Ferroelectricity	206
6.9	Doping and Modification of Properties	208
6.10	Nanoparticles and Thin Films	212
	References	215
	Further Reading	215
7	Magnetic Properties	217
7.1	Magnetism in Perovskites	217
7.2	Paramagnetic Perovskites	219
7.3	Antiferromagnetic Perovskites	222
7.3.1	Cubic Perovskite-Related Structures	222
7.3.2	Hexagonal Perovskites	229
7.4	Ferromagnetic Perovskites	233
7.5	Ferrimagnetic Perovskites	236
7.6	Spin Glass Behaviour	237
7.7	Canted Spins and Other Magnetic Ordering	238
7.8	Thin Films	240
7.9	Nanoparticles	243

7.10	Multiferroic Perovskites	243
	References	246
	Further Reading	246
8	Electronic Conductivity	247
8.1	Perovskite Band Structure: Metallic Perovskites	247
8.2	Metal–Insulator Transitions	250
8.2.1	Titanates and Related Phases	250
8.2.2	LnNiO_3	252
8.2.3	Lanthanoid Manganites	253
8.2.4	Lanthanoid Cobaltites	254
8.2.5	$(\text{Sr}, \text{Ca})_2\text{RuO}_4$ and $\text{Ca}_2\text{Ru}_{1-x}\text{Cr}_x\text{O}_4$	255
8.2.6	NaOsO_3	256
8.3	Perovskite Superconductors	257
8.4	Cuprate High-Temperature Superconductors	258
8.4.1	Overview	258
8.4.2	Lanthanum Cuprate, La_2CuO_4	259
8.4.3	Neodymium Cuprate, Nd_2CuO_4	260
8.4.4	Yttrium Barium Copper Oxide, $\text{YBa}_2\text{Cu}_3\text{O}_7$	261
8.4.5	Perovskite-Related Structures and Series	263
8.4.6	The Generic Superconductivity Phase Diagram	263
8.4.7	Defects and Conductivity	265
8.5	Spin Polarisation and Half-Metals	267
8.6	Charge Ordering and Orbital Ordering	268
8.7	Magnetoresistance	270
8.7.1	Colossal Magnetoresistance (CMR) in Manganites	270
8.7.2	Low-Field Magnetoresistance	272
8.8	Semiconductivity in Perovskites	272
8.9	Thin Films and Surface Conductivity	275
	References	275
	Further Reading	275
9	Thermal and Optical Properties	277
9.1	Thermal Expansion	277
9.1.1	Normal Thermal Expansion	277
9.1.2	Thermal Contraction	280
9.1.3	Zero Thermal Expansion Materials	283
9.2	Thermoelectric Properties	284
9.3	The Magnetocaloric Effect	287

9.4	The Pyroelectric and Electrocaloric Effect	288
9.5	Transparency	289
9.6	Electrochromic Films	291
9.7	Electro-optic Properties	293
9.7.1	Refractive Index Changes	293
9.7.2	Electro-optic Phase Modulators	294
9.7.3	Electro-optic Intensity Modulators	296
9.7.4	Ceramic Modulators	299
9.8	Perovskite Solar Cells	299
	Reference	302
	Further Reading	302
<i>Appendix A The Bond Valence Model for Perovskites</i>		303
<i>Appendix B Summary of the Kröger–Vink Defect Notation</i>		307
<i>Index</i>		309

Preface

Perovskites are a class of compounds with structures related to that of the mineral Perovskite, CaTiO_3 , and can be considered to be derived from a parent phase of general formula ABX_3 . They have been intensively studied since the middle of the twentieth century because of their innate properties: initially dielectric, piezoelectric and ferroelectric. This range of behaviour has been expanded into areas which include magnetic ordering, multiferroic properties, electronic conductivity, superconductivity and thermal and optical properties. Apart from these purely physical aspects, the phases show a wide range of chemical attributes. They are used as electrode materials for solid oxide fuel cells where materials with high oxide ion conductivity, electronic conductivity and mixed ionic/electronic conductivity are required. Many perovskite phases show useful catalytic and redox behaviour, often dependent upon the presence of chemical defects in the phase.

This complexity is a result of two prime factors. Firstly the crystal structures encompassed by the term ‘perovskite’ embrace a huge range, from the simple cubic ‘aristotype’ SrTiO_3 to cation- and anion-deficient phases, modular phases including the cuprate superconductors and hexagonal perovskites related to BaNiO_3 . In addition, both the chemical and physical properties of any member of these structural forms can be tuned over wide ranges by relatively simple substitution into all or some of the A-, B- and X-sites. This wide-ranging flexibility includes the formation of perovskites in which the A cation is replaced by an organic molecule, typified by the perovskite methylammonium lead iodide, now intensely studied as the core of ‘perovskite’ photovoltaic cells. Additionally, the properties of thin films, superlattices and nanoparticles show new and totally unexpected responses, when compared to the behaviour of the separate bulk phases.

The aim of this book is to provide a compact overview of this large body of knowledge. An outline of the structures of these phases is of primary importance as a prerequisite to an understanding of many physical properties. This material is contained in the earlier chapters. For the purposes of providing an overall vista, crystal structures are mostly represented as idealised forms. This has the advantage of bringing out the structural relationships between the phases described, but the obverse side is that it does obscure small details that may be of significance. However, the detailed crystallographic parameters of all the phases mentioned in

this book are available via the CrystalWorks database (<http://www.cds.rsc.org>). This source will also provide literature references to the originally published crystallographic data of all the phases listed. Crystal structures are followed by a survey of physical and chemical properties. The properties emphasised are, where possible, those unique to perovskites or at least manifested in a singular way by these compounds. They are grouped into broad categories – chemical, dielectric, magnetic, electronic, thermal and optical properties – although these classifications cannot truly be cleanly separated from each other.

In a book of modest size, it is necessary to be somewhat selective in material content. For this reason, two areas have been omitted. The first of these concerns preparation techniques. In the main these are the normal techniques of solid-state chemistry, physics and ceramic science and are not unique to perovskites. Secondly catalysis has also been omitted. Again, the bulk of the catalytic reactions studied are not unique to perovskites and are better described and discussed within the broader perspective of catalysis rather than via the narrower standpoint of perovskites.

Although large numbers of papers are published each month detailing some aspect or other of perovskite physics and chemistry, it is felt that an extensive literature reference section would overwhelm any reader seeking a broad overview of the field. Because of this, the Further Reading sections contain mainly reviews or selected recent references that expand material in the text. These are sufficient to provide an entry point to the literature base for those needing additional information. In addition a few sources that explain the basic concepts of crystallography and structure–property relationships are added, and two appendices are included that explain two rather more specialist aspects of nomenclature.

As ever, I am grateful to my wife Anne for support and tolerance during the assembly of this work, without which the project could not have been undertaken. In addition I thank my family for continual encouragement. Finally I am indebted to the staff of the Trevithick Library, University of Cardiff, who helped with literature resources and related matters.

Richard Tilley
January 2016

1

The ABX_3 Perovskite Structure

1.1 Perovskites

Perovskite is a mineral of formula $CaTiO_3$. It was discovered in 1839 by the Prussian mineralogist Gustav Rose in mineral deposits in the Ural Mountains and named after the Russian mineralogist Count Lev Aleksevich von Petrovski. Natural crystals have a hardness of 5.5–6 and a density of $4000\text{--}4300\text{ kg m}^{-3}$. They are usually dark brown to black, due to impurities, but when pure are clear with a refractive index of approximately 2.38. The crystal structure of this compound, initially thought to be cubic, was later shown to be orthorhombic (Table 1.1).

As with many minerals, Perovskite has given its name to a family of compounds called *perovskites*, which have a general formula close to or derived from the composition ABX_3 . At present many hundreds of compounds are known that adopt the perovskite structure. In fact a perovskite structure mineral, Bridgmanite (Fe,Mg) SiO_3 , is the most abundant solid phase in the Earth's interior, making up 38% of the total. The phase occurs between depths of approximately 660–2900 km but is only stable at high temperatures and pressures so that it is not found at the surface of the Earth.

To some extent the multiplicity of phases that belong to the perovskite family can be rationalised by assuming that perovskites are simple ionic compounds, where A is usually a large cation, B is usually a medium-sized cation and X is an anion.

Table 1.1 Representative ABX_3 perovskite phases^a

Phase	Space group ^b	Unit cell		
		<i>a</i> (nm)	<i>b</i> (nm)	<i>c</i> (nm)
1, 2				
AgMgF ₃	<i>C</i> , $Pm\bar{3}m$ (221)	0.41162		
CsPbI ₃	<i>C</i> , $Pm\bar{3}m$ (221)	0.62894		
KCuF ₃	<i>T</i> , $I4/mcm$ (140)	0.56086		0.76281
KMgF ₃	<i>C</i> , $Pm\bar{3}m$ (221)	0.39897		
KZnF ₃	<i>C</i> , $Pm\bar{3}m$	0.40560		
NaMgF ₃	<i>O</i> , $Pbnm$ (62)	0.48904	0.52022	0.71403
NaFeF ₃	<i>O</i> , $Pnma$ (62)	0.56612	0.78801	0.54836
NH ₄ ZnF ₃	<i>C</i> , $Pm\bar{3}m$ (221)	0.41162		
1, 5				
KTaO ₃	<i>C</i> , $Pm\bar{3}m$ (221)	0.40316		
KNbO ₃	<i>O</i> , $Amm2$ (38)	0.3971	0.5697	0.5723
2, 4				
SrTiO ₃	<i>C</i> , $Pm\bar{3}m$ (221)	0.3905		
BaTiO ₃	<i>T</i> , $P4mm$ (99)	0.39906		0.40278
CaTiO ₃	<i>O</i> , $Pbmn$ (62)	0.54035	0.54878	0.76626
BaSnO ₃	<i>C</i> , $Pm\bar{3}m$ (221)	0.4117		
CdSnO ₃	<i>O</i> , $Pnma$ (62)	0.52856	0.74501	0.51927
CaIrO ₃	<i>O</i> , $Pbnm$ (62)	0.52505	0.55929	0.76769
PbTiO ₃	<i>T</i> , $P4mm$ (99)	0.3902		0.4143
PbZrO ₃	<i>O</i> , $Pbam$ (55)	0.58822	1.17813	0.82293
SrCoO ₃	<i>C</i> , $Pm\bar{3}m$ (221)	0.3855		
SrMoO ₃	<i>C</i> , $Pm\bar{3}m$ (221)	0.39761		
SrRuO ₃	<i>O</i> , $Pnma$ (62)	0.55328	0.78471	0.55693
(Fe,Mg)SiO ₃	<i>O</i> , $Pnma$ (62)	0.5020	0.6900	0.4810
3, 3				
BiFeO ₃	<i>Tr</i> , $R3c$ (161)	0.55798		1.3867
BiInO ₃	<i>O</i> , $Pnma$ (62)	0.59546	0.83864	0.50619
ErCoO ₃	<i>O</i> , $Pbnm$ (62)	0.51212	0.54191	0.73519
GdFeO ₃	<i>O</i> , $Pbnm$ (62)	0.53490	0.56089	0.76687
HoCrO ₃	<i>O</i> , $Pnma$ (62)	0.5518	0.7539	0.5245
LaAlO ₃	<i>Tr</i> , $R3c$ (161)	0.53644		1.31195
LaCoO ₃	<i>Tr</i> , $R\bar{3}c$ (167)	0.54437		1.30957
LaMnO ₃	<i>O</i> , $Pbnm$ (62)	0.55367	0.57473	0.76929
LaTiO ₃	<i>O</i> , $Pbnm$ (62)	0.5576	0.5542	0.7587
NdAlO ₃	<i>Tr</i> , $R\bar{3}c$ (167)	0.53796		1.31386
PrRuO ₃	<i>O</i> , $Pnma$ (62)	0.58344	0.77477	0.53794
YbMnO ₃	<i>O</i> , $Pbnm$ (62)	0.52208	0.58033	0.73053
4, 5				
ThTaN ₃	<i>C</i> , $Pm\bar{3}m$	0.4020		

^a Many of these phases are polymorphic, and lattice parameters vary with temperature and pressure.^b The crystal system, here and throughout the other tables in this book, is abbreviated thus: *C*, cubic; *H*, hexagonal; *M*, monoclinic; *O*, orthorhombic; *T*, tetragonal; *Tr*, trigonal (often specified in terms of a hexagonal unit cell); *Tri*, triclinic.

Naturally the overall ionic structure must be electrically neutral. If the charges on the ions are written as q_A , q_B and q_X , then

$$q_A + q_B = -3q_X$$

Frequently encountered (but not exclusive) combinations are

$$\begin{aligned} q_X = -1, \quad (q_A, q_B) &= (1, 2); \text{ for example, } \text{KNiF}_3; \\ q_X = -2, \quad (q_A, q_B) &= (1, 5); \text{ for example, } \text{NaNbO}_3; \\ &\quad (q_A, q_B) = (2, 4); \text{ for example, } \text{CaTiO}_3; \\ &\quad (q_A, q_B) = (3, 3); \text{ for example, } \text{LaAlO}_3; \\ q_X = -3, \quad (q_A, q_B) &= (4, 5); \text{ for example, } \text{ThTaN}_3. \end{aligned}$$

The importance of perovskites became apparent with the discovery of the valuable dielectric and ferroelectric properties of barium titanate, BaTiO_3 , in the 1940s. This material was rapidly employed in electronics in the form of capacitors and transducers. In the decades that followed, attempts to improve the material properties of BaTiO_3 lead to intensive research on the structure – property relations of a large number of nominally ionic ceramic perovskite-related phases with overall compositions ABO_3 , with a result that vast numbers of new phases were synthesised.

It was soon realised that, as a group, these materials possessed very useful physical and chemical properties far broader than those shown by BaTiO_3 , and research widened to include a range of structures and phases that could all be related structurally to the perovskite family, including nominally ionic nitrides and oxynitrides. In addition, a number of materials which are better described as alloys, of formula A_3BX , where A and B are metals and X is an anion or semimetal, typically C, N, O and B are known. These are often said to adopt the so-called *antiperovskite* or *inverse perovskite* structure, because the metal A atoms occupy the positions corresponding to the anions in the ionic perovskites and the B and X atoms occupy sites corresponding to those occupied by the cations. The flexibility of the perovskite framework also allows it to include cations such as NH_4^+ , which can often be considered to be spherical at normal temperatures. More complex phases, such as the inorganic–organic hybrid compounds $(\text{CH}_3\text{NH}_3)\text{PbX}_3$, where X is typically Cl, Br, I or a combination of these anions, have also been synthesised.

As well as phases with an ABX_3 composition, large numbers of modular structures have been prepared, all of which are built up, at least in part, from fragments, usually slabs, of perovskite-like structure. The formulae of these are not easily reconciled with a composition of ABX_3 until the structural building principles have been found and the nature of the interfaces between the various slabs is clarified.

For example, $\text{Bi}_2\text{Ca}_2\text{Sr}_2\text{Cu}_3\text{O}_{10+\delta}$, a superconducting oxide, is built from slabs of perovskite type separated by slabs of composition Bi_2O_2 .

As would be expected, there is a close correlation between chemical and physical properties in these complex materials. It is this flexibility that makes the perovskites as a group, important, as the facile replacement of any of the atoms in this range of structures can be used to modify important physical properties in a controlled way. The flexibility comes at a structural cost. The ABX_3 perovskite structure is beset by structural variations that depend upon exact composition as well as temperature and pressure, all of which have a profound significance for physical properties. Moreover, many multi-cation or anion materials show an intricate microdomain structure when examined by transmission electron microscopy. These microdomains are small volumes of differing structural complexity that exist within a coherent anion matrix. Often they show ordering of atoms over several unit cell volumes with the pattern of order changing from one microdomain to its neighbours. When these microdomains are arranged throughout the crystal in a more or less random fashion, dependent upon the symmetry of the phase, the microscopic ordering is hidden from normal X-ray and neutron diffraction structure solving methods and may not feature in the refined structure of the macroscopic crystal studied. This level of order is generally revealed by high-resolution transmission electron microscopy. Because of this divergence, exact structural details of many perovskite phases of complex composition are open to question, although the overall broad-brush structure is known.

Fortunately much of this diversity can be understood or rationalised in terms of an ideal cubic perovskite structure. In this chapter the ideal ABX_3 perovskite structure is described together with some of the structural variations that occur which have significance for chemical and physical properties and which make precise structure determination a difficult task.

1.2 The Cubic Perovskite Structure: SrTiO_3

The idealised or *aristotype* perovskite structure is cubic and is adopted by SrTiO_3 at room temperature (but not at all temperatures). There are two general ways of listing the atoms in the cubic unit cell. The standard crystallographic description places the choice of origin at the Sr atom:

SrTiO_3 : cubic; $a=0.3905\text{ nm}$, $Z=1$; space group, $Pm\bar{3}m$ (No. 221);

Atom positions: Sr: 1 (a) 0,0,0;

Ti: 1 (b) $\frac{1}{2}, \frac{1}{2}, \frac{1}{2}$;

O: 3 (c) $\frac{1}{2}, \frac{1}{2}, 0$; $\frac{1}{2}, 0, \frac{1}{2}$; $0, \frac{1}{2}, \frac{1}{2}$;

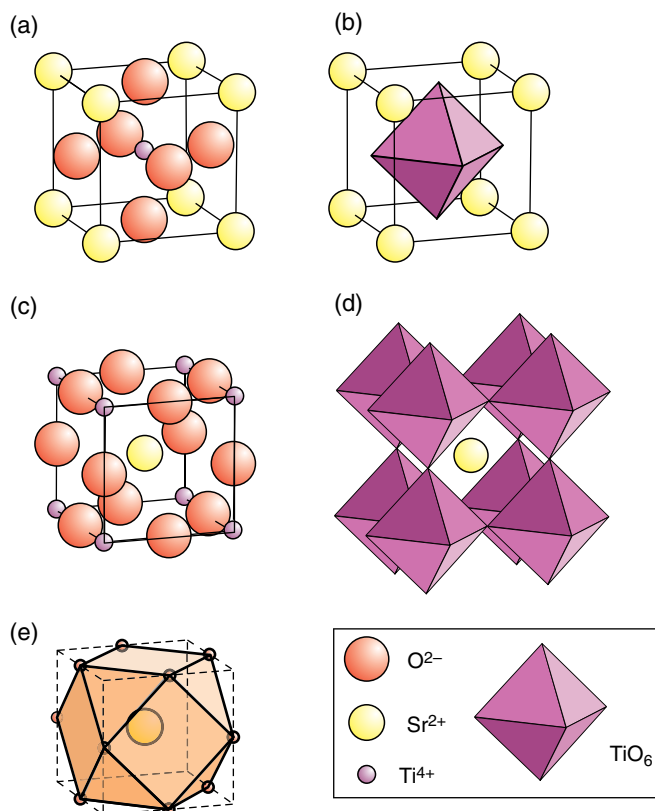


Figure 1.1 The idealised perovskite structure of SrTiO_3 : (a) atom positions with Sr^{2+} at cell origin; (b) TiO_6 octahedral coordination polyhedron; (c) atom positions with Ti^{4+} at cell origin; (d) TiO_6 octahedral polyhedron framework with Sr^{2+} at the cell centre; (e) cuboctahedral cage site

The Sr^{2+} ions lie at the corners of the unit cell. The Ti^{4+} ions lie at the cell centre and are surrounded by a regular octahedron of O^{2-} ions (Figure 1.1a and b). For some purposes it is useful to translate the cell origin to the Ti^{4+} ions:

$$\begin{aligned}\text{Atom positions : Ti : } &1(a)0,0,0; \\ &\text{Sr : }1(b)\frac{1}{2},\frac{1}{2},\frac{1}{2}; \\ &\text{O : }3(d)\frac{1}{2},0,0; 0,\frac{1}{2},0; 0,0,\frac{1}{2};\end{aligned}$$

The large Sr^{2+} ions are coordinated to 12 O^{2-} ions and are now situated at the unit cell centre (Figure 1.1c). For a discussion of the chemical and physical properties of this (and other) perovskites, it is convenient to think of the structure as built-up from an array of corner sharing TiO_6 octahedra (Figure 1.1d). The large Sr^{2+} ions are located at

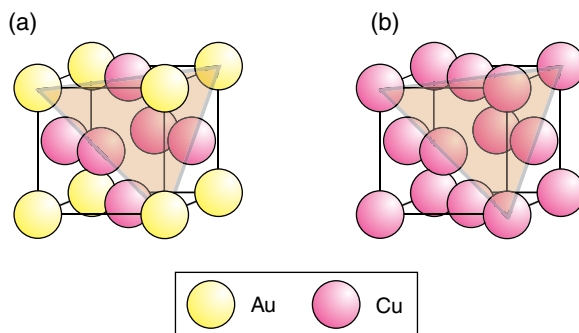


Figure 1.2 (a) The AuCu_3 and (b) the Cu (A1, fcc) structure

the unit cell centre and are surrounded by a cuboctahedral cage of O^{2-} ions (Figure 1.1e). The TiO_6 framework is regular and the octahedra are parallel to each other. All the $\text{Ti}^{4+}\text{—O}^{2-}$ bond lengths are equal and the six $\text{O}^{2-}\text{—Ti}^{4+}\text{—O}^{2-}$ bonds are linear.

The Sr^{2+} and O^{2-} positions in the SrTiO_3 structure are identical to that of the Au and Cu positions in the alloy Cu_3Au , and if the difference between the Sr^{2+} and O^{2-} ions (or Cu and Au atoms) is ignored, they form a cubic array identical to that of the Cu structure (Figure 1.2a and b). This latter is the simple A1 structure type, often described as the face-centred cubic (fcc) structure, which is made up of (111) planes that lie normal to the cell body diagonal [111], stacked in the normal face-centred sequence ... ABCABC.... Thus the SrTiO_3 structure can also be thought of as a built-up from close-packed layers of (111) planes containing ordered Sr^{2+} and O^{2-} ions that lie normal to the cubic unit cell body diagonal [111]. The charge balance needed to maintain charge neutrality in this skeleton structure is provided by an ordered distribution of the Ti^{4+} ions in the available octahedral interstices that are bounded by O^{2-} ions only (Figure 1.3).

It is often convenient when describing the structures of more complex perovskite-related phases (Chapters 2 and 3) to display the structure as linked ideal TiO_6 octahedra. The conventional view of the ideal perovskite structure (Figure 1.4a) is often shown tilted to make the (111) layers almost or exactly horizontal (Figure 1.4b and c). More often the alkaline earth atoms are omitted and just the octahedral framework is shown (Figure 1.4d and e). Other projections, such as down [111], show the octahedra projected as hexagonal outlines or down [110] as diamond outlines (Figure 1.4f and g).

1.3 The Goldschmidt Tolerance Factor

From a crystallographic perspective, the ideal perovskite structure is inflexible, as the unit cell has no adjustable atomic position parameters, so that any compositional change must be accommodated by a change in lattice parameter. This is a

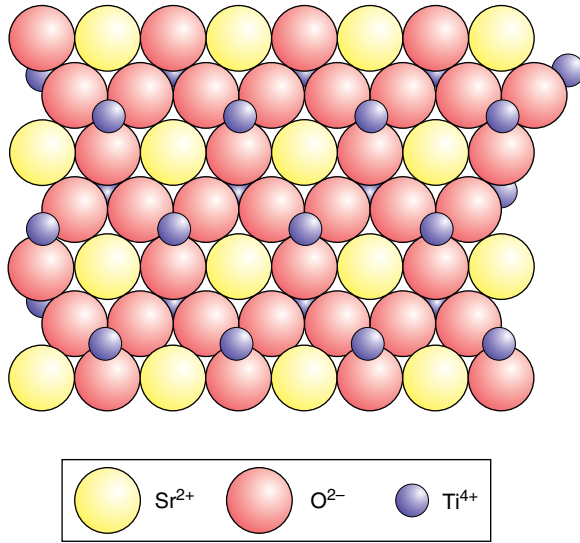


Figure 1.3 A single SrO_3 (111) plane in $SrTiO_3$. The Ti^{4+} ions, above and below the SrO_3 layer, occupy octahedral interstices that are bounded by six O^{2-} ions

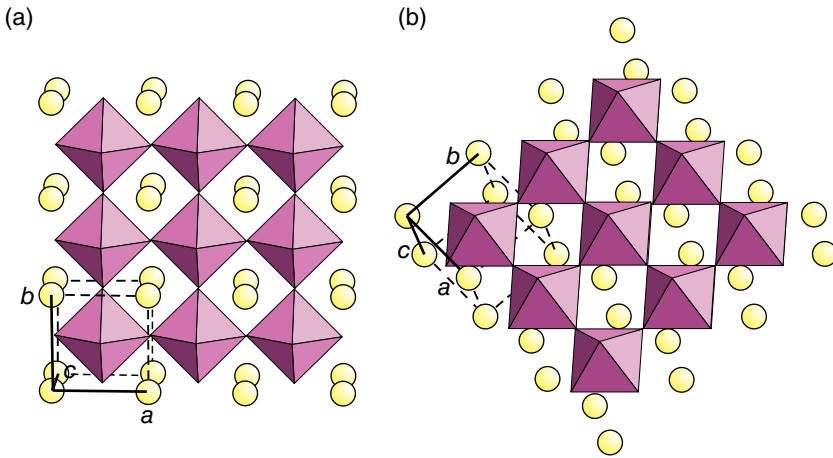
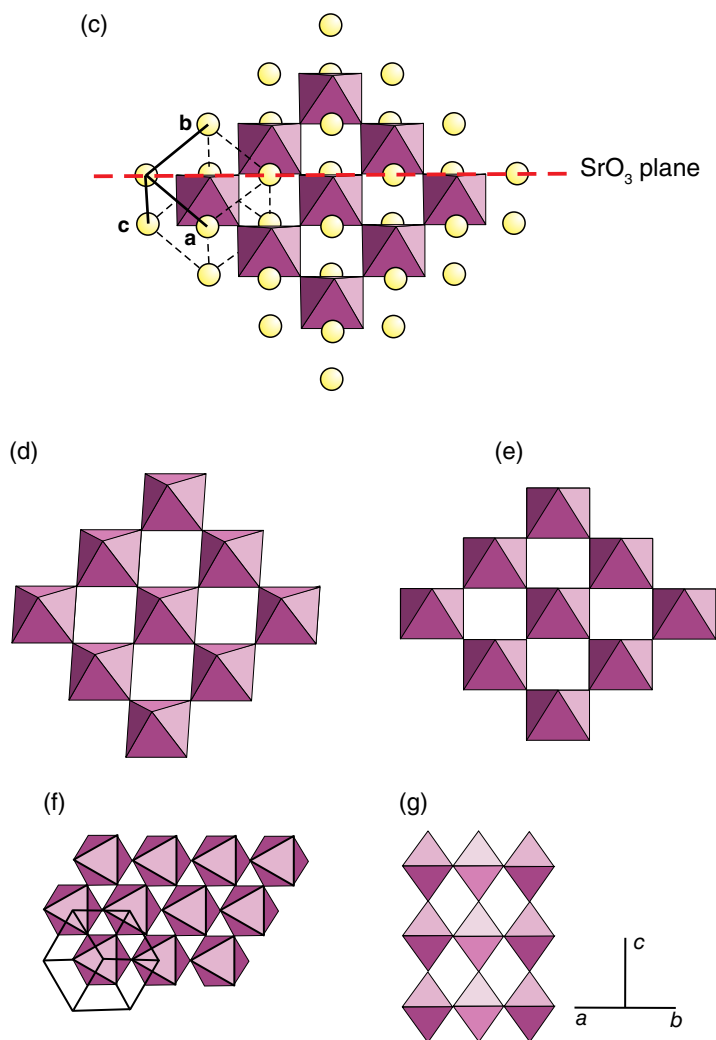


Figure 1.4 The cubic $SrTiO_3$ perovskite structure (a) conventional view with $3 \times 3 \times 1$ unit cells displayed; (b) the same rotated by approximately 45° ; (c) the same rotated further so that one set of SrO_3 planes lies normal to the plane of the page; (d and e) as (b and c) showing only the TiO_6 octahedral framework; (f) octahedral framework projected down $[111]$; (g) octahedral framework projected down $[110]$

**Figure 1.4** (Continued)

simple sum of anion – cation bond lengths. The cubic unit cell edge, a , is equal to twice the B–X bond length:

$$2(\text{B} - \text{X}) = a$$

The width of the cuboctahedral cage site, $\sqrt{2}a$, is equal to twice the A–X bond length:

$$2(\text{A} - \text{X}) = \sqrt{2}a$$

This means that the ideal structure forms when the ratio of the bond lengths is given by:

$$\frac{(A-X)}{(B-X)} = \sqrt{2}$$

or

$$\frac{(A-X)}{\sqrt{2}(B-X)} = 1$$

This relationship was first exploited by Goldschmidt, in 1926, who suggested that it could be used to predict the likelihood that a pair of ions would form a perovskite structure phase. When this was initially proposed, very few crystal structures had been determined and so ionic radii were used as a substitute for measured bond lengths. For this purpose, it is assumed that for a stable structure to form the cations, just touch the surrounding anions (Goldschmidt's rule), then:

$$\frac{(r_A + r_X)}{(r_B + r_X)} = \sqrt{2}$$

or

$$t = \frac{(r_A + r_X)}{\sqrt{2}(r_B + r_X)} = 1 \text{ (ideal structure)}$$

where t is called the *tolerance factor*, r_A is the radius of the cage site cation, r_B is the radius of the octahedrally coordinated cation and r_X is the radius of the anion. Goldschmidt's proposal was that a perovskite structure phase would form if the value of the tolerance factor, t , was close to 1.0.

Note that it is necessary to use ionic radii appropriate to the coordination geometry of the ions. Thus r_A should be appropriate to 12 coordination, r_B to octahedral coordination and r_X to linear coordination. Furthermore, it is best to use radii scales that mirror the X anion present, as radii appropriate to oxides, although a reasonable approximation for fluorides, are poor when applied to chlorides and sulphides.

Because many perovskite structures have been described, it is now usual to use the measured bond lengths in the crystal rather than ionic radii to give an *observed tolerance factor* t_{obs} :

$$t_{\text{obs}} = \frac{(A-X)}{\sqrt{2}(B-X)}$$

where $(A-X)$ is the average of the measured bond lengths between the A cation and the surrounding 12 anions and $(B-X)$ is the average of the measured bond lengths between the B cation and the surrounding six anions. It is found that for specific groups of perovskites (e.g. $ATiO_3$ titanates, AlO_3 aluminates), there is a linear relationship between t_{obs} and t which varies slightly from one family to another.

Despite its simplicity, the tolerance factor has reasonable predictive power, especially for oxides, where ionic radii are known with greatest precision. Ideally t should be equal to 1.0 and it has been found empirically that if t lies in the approximate range 0.9–1.0 a cubic perovskite structure is a reasonable possibility. If $t > 1$, that is, large A and small B, a hexagonal packing of the AX_3 layers is preferred and hexagonal phases of the $BaNiO_3$ type form (Chapter 3). In cases where t of the order of 0.71–0.9, the structure, particularly the octahedral framework, distorts to close down the cuboctahedral coordination polyhedron, which results in a crystal structure of lower symmetry than cubic. For even lower values of t , the A and B cations are of similar size and are associated with the ilmenite, $FeTiO_3$, structure or the C-type rare earth Ln_2O_3 structure.

In the case of chlorides and sulphides, the tolerance factor tends to move downwards compared to that for oxides and fluorides so that cubic and distorted cubic phases form for t in the range 0.8–0.9, and hexagonal perovskites form if t is greater than 0.9.

The concept of the tolerance factor can be extended to perovskites with more complex compositions by using an average value for ionic radii or bond length. For example, for an A-site substituted phase $A_{1-x}A'_xBX_3$, one can write

$$t = \frac{[(1-x)r_A + xr_{A'} + r_X]}{\sqrt{2}(r_B + r_X)}$$

and in the case of B-site substitution $AB_{1-x}B'_xX_3$:

$$t = \frac{(r_A + r_X)}{\sqrt{2}[(1-x)r_B + xr_{B'} + r_X]}$$

Similarly, in terms of bond lengths:

$$t_{\text{obs}} = \frac{\langle A-X \rangle}{\sqrt{2} \langle B-X \rangle}$$

where $\langle A-X \rangle$ signifies the average bond length for the links $A-X$, $A'-X$, etc. and $\langle B-X \rangle$ signifies the average bond length for the links $B-X$, $B'-X$, etc. Both equations can be generalised to more complex structures $(A, A', A'' \dots) (B, B', B'' \dots) (X, X', X'' \dots)_3$.

1.4 ABX_3 Perovskite Structure Variants

The BX_6 octahedra are the root of many of the important physical properties of perovskites, such as magnetic and ferroelectric responses to external fields. This is because these are often mediated by the electron configurations of the B cations, which themselves are modified by the surrounding geometry of the six anions. The A cations, although they cannot be ignored, tend to be closed-shell ions with a fixed valence and so less responsive to chemical manipulation with a view to modification of chemical and physical properties. Thus it is useful to place the distortions that occur in perovskites due to the shape and relative orientation of the BX_6 polyhedra into a crystallographic framework.

The simplest change that can be envisaged is that in which the BX_6 octahedra remain perfect (or nearly so) and the cations are simply displaced away from the centre of the octahedron. Cation displacement is usually associated with cations that are ‘too small’ for the octahedral site, leading to a tolerance factor significantly less than 1 (although in fact B-cation size is only one of several factors of importance in this distortion). The structure now becomes tetragonal, trigonal or orthorhombic, depending upon the direction of cation displacement and the magnitude of the displacements which occur. In addition, the displacements produce permanent electric dipoles in the unit cell and can give rise to pyroelectric, ferroelectric and antiferroelectric effects (Chapter 6).

A second structural response which preserves the perfect (or nearly perfect) BX_6 octahedral geometry is octahedral tilt or rotation. This response is mostly associated with A cations that are too small for the cuboctahedral cage site, and so the BX_6 octahedra twist so as to effectively reduce the cavity dimensions, again allowing the structure to accommodate values of t less than 1. As with cation displacement, rotation also lowers the symmetry of the crystal (Section 1.7) and has a profound influence on the physical properties of these phases.

Finally, the BX_6 octahedron itself can distort to give elongated or flattened octahedra, which in extreme cases can lead to square planar or square pyramidal coordination. These distortions are a result of interactions between the cation electron orbitals and the surrounding anions, typified by the Jahn–Teller effect (Section 1.6). Octahedral distortion can also be caused by cation valence changes such as disproportionation:



The two different-sized cations then may adjust to the surroundings by a distortion of one or both of the cation-centred BX_6 octahedra to give rise to two different-sized octahedra.

These three modifications, namely, B-cation displacement, BX_6 tilt/rotation and BX_6 distortion, are not mutually exclusive and they can occur independently or, often, in combination with one another. Moreover, the resulting changes may be cooperative in that they affect all octahedra in a similar way, or non-cooperative, in which case the distortions may cancel out at a macroscopic level although they may still influence microscopic properties.

The amounts of distortion are generally small and are readily influenced by the ambient conditions. Thus changes in temperature, pressure, crystallite size or form may alter the degree of distortion or the type of distortion present. The majority of perovskite phases manifest a series of symmetry changes as the temperature or pressure is changed, usually resulting in a cubic form at higher temperatures and pressures. For example, the perovskite SrSnO_3 , which is orthorhombic, space group $Pmna$, at room temperature, changes as the temperature increases to orthorhombic, space group $Imma$, at 905 K, to tetragonal, space group $I4/mcm$ at 1062 K and finally to cubic space group $Pm\bar{3}m$ at 1295 K.

For many of these lower symmetry forms, the shift from the ideal cell is small or can be neglected for some purposes, and in such cases it is often convenient to refer these structures to an idealised pseudocubic structure, of cell length a_p (equivalent to a for ideal SrTiO_3 , 0.39 nm), that can be used as a first (and often sufficient) approximation in describing the properties of the phases.

1.5 Cation Displacement: BaTiO_3 as an Example

Cation displacement in BaTiO_3 is attributed to the second order (or pseudo) Jahn–Teller effect, acting upon the $d^0 \text{Ti}^{4+}$ ion. This mechanism applies to nonlinear molecules with a nondegenerate electronic ground state accompanied by a very low-lying excited state. Under these conditions, distortions of symmetry occur that facilitate the mixing of the electronic ground and excited states in a way to lower the ground-state energy. In perovskites, the appropriate symmetry change is provided by cation displacement. (The first-order Jahn–Teller effect, which affects d^n cations, is described in Section 1.6.)

To preserve a maximum degree of symmetry, cation displacement needs to be along one of the symmetry axes of the octahedron. There are three tetrad (fourfold) axes of rotational symmetry, each passing through opposite vertices of the octahedron; four triad (threefold) axes of rotational symmetry, each passing through the centres of opposing triangular faces of the octahedron and six diad (twofold) axes

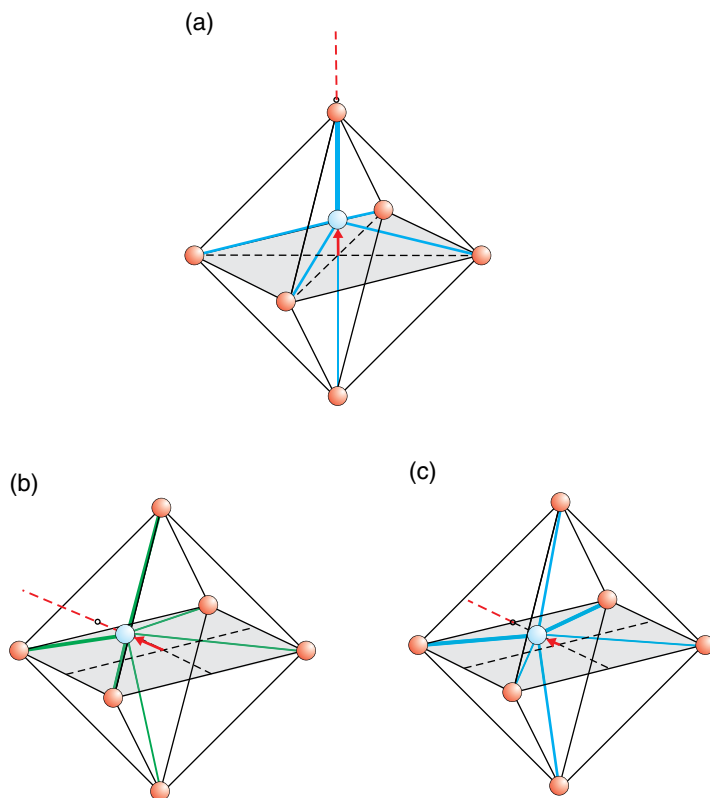


Figure 1.5 Cation displacement in a BX_6 octahedron: cation displacement along (a) a tetrad axis; (b) a triad axis; (c) a diad axis

of rotational symmetry, each passing through the centres of opposite edges of the octahedron (see Figure 1.10). The symmetry axis parallel to the direction of the displacement is maintained after the displacement. Cation displacement parallel to one of the tetrad axes ideally gives rise to one longer bond, one shorter bond and four bonds of intermediate length (Figure 1.5a). Cation displacement along a triad axis ideally gives rise to three shorter bonds and three longer bonds (Figure 1.5b), while cation displacement along a diad ideally gives rise to two long and two short bonds in the plane containing the diad and two bonds of intermediate length roughly perpendicular to that plane (Figure 1.5c). The simplest structures are found when all of the cation displacements are identical and in such cases, B-cation displacement is usually accompanied by smaller A-cation displacement.

The effects of B-cation displacement upon the structures and dielectric properties of perovskite phases have been extensively studied in the important dielectric/ferroelectric perovskite, $BaTiO_3$. The phase shows transformations from trigonal to

orthorhombic (at 183 K), orthorhombic to tetragonal (at 263 K) and tetragonal to cubic (at 393 K), all due to cation displacement.

The high-temperature phase, stable above 393 K, adopts the ideal perovskite structure: space group $Pm\bar{3}m$ (221), $a=0.39732$ nm (Figure 1.6a). The medium-sized Ti^{4+} ions are situated at the centre of an octahedron of oxygen ions with equal bond lengths of approximately 0.2 nm, while the large Ba^{2+} cations are in the centres of the cuboctahedral cage sites, surrounded by 12 oxygen ions.

Between 393 and 268 K the unit cell is tetragonal and ferroelectric. As the crystal cools through the cubic – tetragonal transition temperature, the cubic cell expands slightly along one edge to produce the tetragonal **c**-axis and is slightly compressed along the other two edges to form the tetragonal **a**- and **b**-axes: space group $P4mm$ (99). $a=b=0.39910$ nm, $c=0.40352$ nm (Figure 1.6b). The change from cubic to tetragonal is accompanied by an off-centre movement of the octahedrally coordinated Ti^{4+} ions along the +**c**-axis, which is one of the tetrad axes of the octahedron (Figure 1.6c). The $\text{O}^{2-}\text{--Ti}^{4+}$ bond lengths parallel to the **c**-axis are now ≈ 0.22 and ≈ 0.18 nm, while the equatorial bond lengths remain at ≈ 0.2 nm. The change in the Ba^{2+} positions is almost negligible. The Ti^{4+} displacement is accompanied by a slight change in octahedron dimensions so that two equatorial oxygen atoms move parallel to the +**c**-axis and two move in the opposite direction. These displacements give rise to electric dipoles, p , one in each octahedron (Figure 1.6d) that are the source of the ferroelectric properties of tetragonal BaTiO_3 . There is no preference as to which of the original cubic axes becomes the polar direction, and so this can take one of six equivalent directions, so that a single crystal invariably becomes heavily twinned on cooling.

Between the temperatures 263 and 183 K, the tetragonal structure undergoes a further transition with the Ti^{4+} cation displaced along a diad axis (Figure 1.6e) giving four $\text{Ti}\text{--O}$ bonds approximately 0.198 nm and two bonds approximately 0.201 nm in length, with once again a slight distortion of the octahedra, producing an ordered array of electronic dipoles. This results in an elongation along a face diagonal of the pseudocubic unit cell to give an orthorhombic phase: space group $Amm2$ (38), $a=0.39594$ nm, $b=0.56266$ nm, $c=0.56435$ nm (Figure 1.6f).

Below 183 K the Ti^{4+} cation displacement is along the triad axis, giving rise to three shorter $\text{Ti}\text{--O}$ bonds of approximately 0.21 nm and three bonds of ≈ 0.19 nm in length (Figure 1.6g). The pseudocubic cell is now elongated along the cell body diagonal to produce a rhombohedral cell: space group $R3m$ (160), $a=0.40043$ nm, $\alpha \approx 89.86^\circ$ (Figure 1.6h). This cell is very close in dimensions to the cubic high-temperature structure but again displays a ferroelectric response to applied electric fields, which the cubic phase does not.

All of the phases described and the cations displacements and octahedral distortions are temperature and pressure sensitive. The phase diagram for BaTiO_3 at

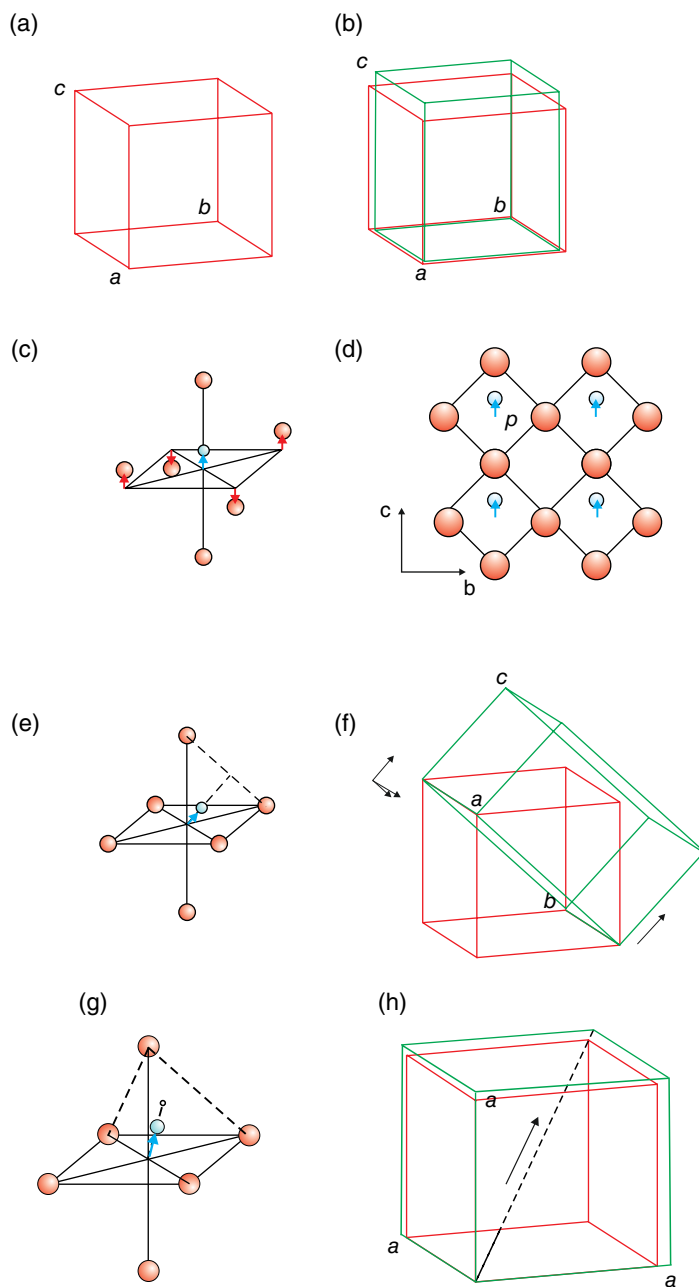


Figure 1.6 Cation displacements (exaggerated for clarity) in BaTiO_3 : (a) $T > 398\text{ K}$, cubic; (b) $398 > T > 278\text{ K}$, tetragonal; (c) ion displacements in each TiO_6 octahedron; (d) electric dipoles generated by Ti^{4+} ion displacements; (e) Ti^{4+} ion displacement in the orthorhombic phase; (f) orthorhombic unit cell compared cubic unit cell; (g) Ti^{4+} ion displacement in the trigonal phase; (h) rhombohedral unit cell compared to cubic unit cell

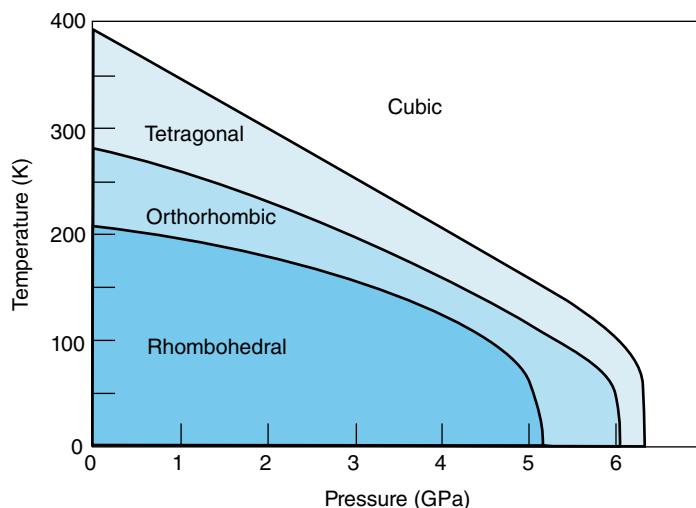


Figure 1.7 The temperature–pressure phase diagram of BaTiO_3 (Original data in Hayward and Salje (2002) and Ishidate et al. (1997))

moderate temperatures and pressures illustrates the symmetry changes encountered (Figure 1.7). It is seen that, at 300 K and ambient pressure (1 atm = 0.000101 GPa), BaTiO_3 will exist as the tetragonal form. When the applied pressure reaches approximately 2 GPa, both the cubic and tetragonal forms will coexist. A slight increase in either pressure or temperature will tip the balance in favour of the cubic form, which will then exist alone.

Note that these changes are also influenced by particle size and morphology. Nanoparticles often present a different pattern of crystallographic behaviour than that illustrated.

1.6 Jahn–Teller Octahedral Distortion: KCuF_3 as an Example

The best known examples of octahedral distortion in perovskites are Jahn–Teller distortions. These arise from the (first order) Jahn–Teller effect, which, in the broadest sense, applies to all nonlinear molecules. The Jahn–Teller theorem says that a molecule with a symmetrical atomic configuration and a degenerate electronic ground state is unstable and will distort so as to remove the electronic degeneracy. With respect to perovskite structures, the Jahn–Teller theorem applies to octahedrally coordinated transition metal B-site cations. It implies that perovskites containing ions with certain d-electron configurations (so-called Jahn–Teller ions) will have an enhanced stability when located in

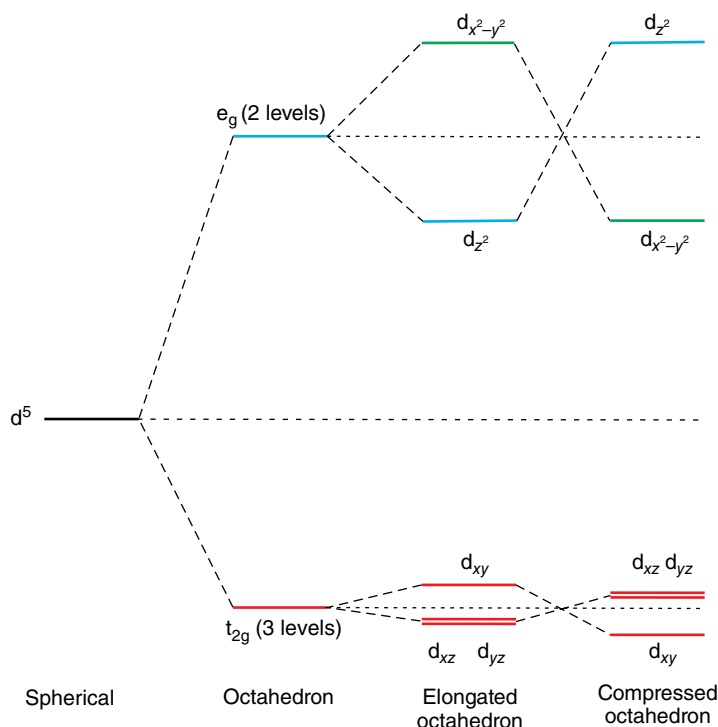


Figure 1.8 The effect of a Jahn–Teller distortion on the d-electron energy levels of a B-site cation in an octahedron

a distorted octahedral environment compared to that in an undistorted one. The distortion may take the form of an elongation of each octahedron along one of its fourfold tetrad symmetry axes, giving a coordination polyhedron with four shorter B–X bonds and two longer B–X bonds or the converse, with four longer B–X bonds and two shorter B–X bonds, leading to a compressed octahedron.

The degenerate ground state comes about in the following way. In an ideal octahedron the d-electron energy levels split into two groups, a lower energy triply degenerate pair, labelled t_{2g} , consisting of the d_{xy} , d_{yz} and d_{xz} orbitals, and an upper doubly degenerate pair labelled e_g , consisting of the orbital pair $d_{x^2-y^2}$ and d_{z^2} (Figure 1.8). A transition metal ion with an odd number of electrons in the upper (e_g) pair of d orbitals, such as high-spin Cr^{2+} , Mn^{3+} (d^4 , $t_{2g}^3 e_g^1$); low-spin Co^{2+} , Ni^{3+} (d^7 , $t_{2g}^6 e_g^1$) and Cu^{2+} (d^9 , $t_{2g}^6 e_g^3$) will have a degenerate ground state because there are a two equivalent electron distributions possible. For example, with Mn^{3+} one electron can be placed in either the $d_{x^2-y^2}$ or d_{z^2} orbital to give the degenerate energy configurations $t_{2g}^3 d_{x^2-y^2}^1 d_{z^2}^0$ or $t_{2g}^3 d_{z^2}^1 d_{x^2-y^2}^0$. The same degeneracy will occur for the

other ions listed. An elongation or compression of the octahedron will remove the degeneracy by a further splitting of the both the t_{2g} and e_g groups (Figure 1.8). The change in the t_{2g} group is rather small and is not of greatest importance for perovskites. The splitting of the e_g group is, however, significant and does lead to octahedral distortion. It is not possible to determine from these qualitative descriptions whether the favoured distortion will be octahedral elongation or compression, but by far the commonest in perovskites is an elongation of the octahedron, which in extreme cases can give rise to square pyramidal or square planar coordination.

In general the A and B ions remain in the centres of the coordination polyhedra in spite of the distortion, but the symmetry of the unit cell drops to tetragonal or orthorhombic. The distortion is both temperature and pressure sensitive, and perovskites showing Jahn–Teller distortion generally return to cubic symmetry at higher temperatures and pressures.

An example that has been investigated in detail is KCuF_3 , containing the Jahn–Teller ion Cu^{2+} . Here the electronic energy level degeneracy in a perfect octahedron corresponds to the alternative electron distributions $d_{x^2-y^2}^2 d_{z^2}^1$ or $d_{x^2-y^2}^1 d_{z^2}^2$. The Jahn–Teller distortion is apparent in the elongated form of the CuF_6 octahedra.

KCuF_3 : tetragonal; $a=b=0.58550\text{ nm}$, $c=0.78456\text{ nm}$, $Z=4$; space group, $I4/mcm$ (No. 140), at 295 K and normal pressure;

Atom positions: Kr: 4 (a) $0,0,\frac{1}{4}; 0,0,\frac{3}{4};$
 Cu: 4 (d) $0,\frac{1}{2},0; \frac{1}{2},0,0;$
 F1: 4 (b) $0,\frac{1}{2},\frac{1}{4}; \frac{1}{2},0,\frac{1}{4};$
 F2: 8 (h) $x, x+\frac{1}{2},0; -x,-x+\frac{1}{2},0; -x+\frac{1}{2},x,0; x+\frac{1}{2},-x,0;$
 $x=0.2281$

The CuF_6 octahedra have one axis elongated to give a Cu–F bond length of 0.225 nm, while the other two are shortened unequally to 0.196 and 0.189 nm (Figure 1.9a and b). The sheets of octahedra lie on planes at $z=0$ and $z=\frac{1}{2}$. All are positioned so that one of the short diameters lies parallel to $[001]$, but within any one sheet of structure parallel to (001) , the long dimensions are arranged so that they lie perpendicular to those of the neighbouring octahedra (Figure 1.9c). The perovskite pseudocubic cell has dimensions $a_p = a/\sqrt{2} = c/2 \approx 0.40\text{ nm}$.

The distortion varies with temperature and pressure in a uniform way. When the pressure increases to 8 GPa, the four shorter bonds become almost equal in length and the long bonds shorten considerably to give an approximately regular octahedral coordination polyhedron.

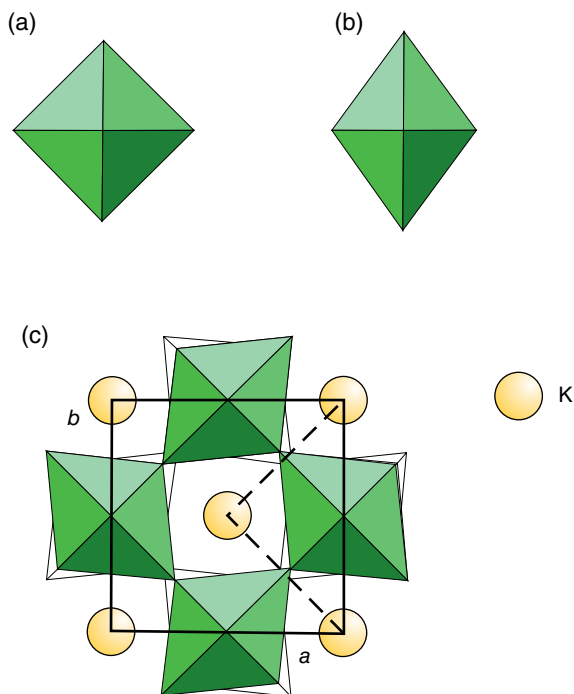


Figure 1.9 The $KCuF_3$ structure: (a) a regular CuO_6 octahedron; (b) CuO_6 octahedron elongated along one tetrad axis; (c) the $KCuF_3$ structure projected down $[001]$. The distorted octahedra in the lower layer are shown in outline, and those in the upper layer are shown shaded. The unit cell is outlined and the pseudocubic cell is dotted

1.7 Octahedral Tilting

1.7.1 Tilt Descriptions

The (ideally rigid) apex-linked BX_6 octahedra can be imagined to be joined by flexible hinges that allow for a certain amount of rotation or tilting. In many cases, slight tilting of the octahedra, so as to enhance stability, is associated with A cations that are slightly too small to fit the ideal structure, as in the example of perovskite, $CaTiO_3$, itself, which displays an orthorhombic symmetry compared to cubic $SrTiO_3$. The tilting contrives to reduce the size of the A-site cavity slightly and so is a mechanism of compensation for a mismatch in the A–X/B–X bond lengths. Tilting can occur about the (a) tetrad, (b) diad and (c) triad axes of the octahedron (Figure 1.10).

The corner connectivity of the BX_6 octahedra means that the tilt of one octahedron completely determines the tilting in the plane perpendicular to the tilt axis